



Comparative studies of the photocatalytic and microwave –assisted degradation of alizarin red using ZnO/poly(1- naphthylamine) nano hybrids



Ufana Riaz ^{*}, S.M. Ashraf ¹, Vaibhav Budhiraja, Sadaf Aleem, Jyoti Kashyap

Materials Research Laboratory, Department of Chemistry, Jamia Millia Islamia (A central University), New Delhi -110025, India

ARTICLE INFO

Article history:

Received 1 November 2015

Received in revised form 4 January 2016

Accepted 6 January 2016

Available online xxxx

Keywords:

Microwave irradiation

Water remediation

Nanohybrid

Photocatalyst

Dye degradation

ABSTRACT

Semiconductors such as ZnO and TiO₂ have been extensively utilized in the photocatalytic degradation of dyes. However till date, no study has been reported to compare the catalytic efficiency of such organic–inorganic hybrids under UV light and microwave irradiation separately. The present work reports the synthesis of poly(1-naphthylamine)/ZnO nano hybrids. The structure and morphology of the synthesized nanocomposites were characterized using FT-IR, UV, XRD, TEM and Cyclic voltammetry analyses. The dye degradation studies were done separately in a photochemical reactor and in laboratory microwave oven and the fragments were identified using LC–MS technique. Results showed that under microwave irradiation, the efficiency of ZnO/PNA as catalyst was higher as compared to UV irradiation. Higher extent of •OH radical generation was confirmed in microwave as compared to UV irradiation which was found to be responsible for the high rate of degradation of dye solution. A plausible degradation pathway was proposed.

© 2016 Elsevier B.V. All rights reserved.

1. Introduction

Semiconductor based photocatalysis has attracted considerable attention for combating environmental pollution [1–3]. Among various inorganic oxides used for photocatalysis, ZnO is one of the most widely investigated semiconductors due to its abundance, low cost as well as low toxicity [4–8]. Although ZnO has been widely reported to be a better photocatalyst than TiO₂ in terms of being less toxic and eco-friendly, its practical utilization is not satisfactory on large scale due to high rate of recombination of the photogenerated charge carriers [9–10]. Hence, the development for a ZnO based photocatalyst with a high charge transfer rate and good separation efficiency is a challenging task. Lately, the combination of inorganic semiconductors with conjugated polymers such as polyaniline (PANI) for enhancing photocatalytic activity has been extensively reported and has shown to remarkably enhance the photocatalytic activity due to its slow charge recombination rate in electron-transfer processes, and good thermal stability [11–13]. Conducting polymers act as sensitizing agents for metals/semiconductor nanoparticles [14–15].

Recently, microwave heating has been utilized as an efficient technique for the fabrication of nanomaterials. Compared with other conventional solution-phase synthetic methods, microwave hydrothermal/solvothermal synthesis provides higher reaction rates at low reaction

temperatures in a very short reaction time, along with good yield [16–20]. Microwave heating processes have been established to produce high-quality ZnO and many studies on the microwave-assisted synthesis of ZnO have revealed a variety of morphologies, such as hollow structures [21], nanorods [22], and self-assembled architectures [23] which have been reported to exhibit remarkable photocatalytic performances.

Microwave-assisted degradation of organic pollutants has also gained momentum lately as a nontoxic and facile technique for the rapid degradation of recalcitrants. Horiskoshi *et al.* [24] have reported that photochemical reactions can be indirectly driven by microwaves using the UV light (180–400 nm) emitted under microwave radiation from microwave discharge electrodeless lamps (MDELs). They have used microwave electrodeless lamp (MWL) as light source for microwave-assisted degradation of azo dyes such as Acid Orange 7 (AO7), bisphenol A and Rhodamine B dye using TiO₂ [25–28]. However, the catalytic activity of ZnO under microwave irradiation alone has not been reported till date. In order to compare and explore the efficiency of ZnO as a microwave catalyst and as a photocatalyst, the present work reports the synthesis of poly(1-naphthylamine)/ZnO nanocomposites. Poly(1-naphthylamine) (PNA) is a well investigated polyaniline derivative and its catalytic efficiency has been reported by our group in our previous works [29–31]. To enhance the catalytic properties of ZnO, its nano hybrids with poly(1-naphthylamine) were formulated using varying ratios of the former and characterized using FTIR, UV–visible, XRD, TEM and cyclic voltammetry studies. Alizarin Red (AR) was chosen as a model dye for the degradation studies which were carried out in a photochemical reactor and a laboratory microwave oven. LC–MS was

^{*} Corresponding author.

E-mail address: ufana2002@yahoo.co.in (U. Riaz).

¹ Now retired.

done to analyze the fragments produced in both processes. Our results revealed that microwave-assisted degradation resulted in products of very low molar mass and low toxicity as compared to the photocatalytic degradation which could be utilized as an eco-friendly technique for the rapid degradation of harmful organic pollutants.

2. Experimental

2.1. Materials

Alizarin Red (AR) dye was procured from S.D.Fine Chem. Pvt. Ltd., India, and used without further purification. 1-Naphthylamine (Sigma Aldrich, USA), zinc oxide (Sigma Aldrich, USA), ferric chloride (Sigma Aldrich, USA), N-methyl-2-pyrrolidone (NMP) (Merck India) were also used without further purification.

2.2. Synthesis of PNA

1-naphthylamine monomer (10 g, 0.069 mol) was added to a 100 ml conical flask containing ethanol and water 1:1 v/v (50 ml each). Ferric chloride (8 g, 0.049) was added to the reaction mixture keeping the monomer: oxidant ratio 1:1.4. The colour of the solution changed from purple to blue indicating rapid polymerization of the monomer. The flask was then kept in an ultrasonicator maintained at 30 °C. The reaction was carried out for 2 h. The synthesized PNA was then taken out and washed several times with distilled water/ethanol on a Buchner funnel. The removal of oxidant was ensured by testing the filtrate with potassium ferrocyanide. PNA was then dried in vacuum oven for 72 h at 70 °C to ensure complete removal of water and impurities.

2.3. Synthesis of ZnO/PNA nanocomposites

For the synthesis of 1 wt% ZnO/PNA nanocomposite, ZnO (0.09 g, 0.0112 mol) and PNA (0.9 g, 0.005 mol) were added to a 100 ml

conical flask containing methanol and water (1:1) 50 ml each. The flask was then kept in an ultrasonicator for 2 h. The synthesized ZnO nanocomposite was taken out then washed with distilled water on a Buchner funnel was then dried in vacuum for 72 h at 70 °C to ensure complete removal of water. Similarly 3 wt% and 5 wt% nanocomposites were prepared and designated as 3-ZnO/PNA and 5-ZnO/PNA. The synthesized nanocomposites were purified by dissolving in THF (80 ml) while stirring on a magnetic stirrer for 6 h to separate the unreacted monomer and oxidant. The mixture was then centrifuged at 6000 rpm for 30 min and the nanocomposite was recovered via precipitation in n-hexane.

2.4. Degradation studies of AR dye solution in microwave and photochemical reactor

AR dye of concentration 250 mg/L, was prepared in distilled water by dilution of a stock solution of 500 mg/L and was labelled as AR-250. It was shaken for one hour in the dark for establishing equilibrium and was irradiated at 30 °C in microwave oven model Ladd Research Microwave oven model LBP-250, USA, fitted with a time and temperature controller. The solution was exposed to microwave irradiation in a batch process for 5, 10, 20, 30 and 40 min. All the experiments were repeated by adding 200 mg of PNA and ZnO/PNA nanocomposite in 100 ml of AR-250 dye solution. The degradation studies carried out under UV irradiation were done in a photochemical reactor (model LELESIL), fitted with a UV lamp of LP250W, Lamp Arc: 125 mm with Built in Resister, Wavelength Spectrum: 200–1100 nm. The lamp was switched on to initiate the photocatalytic degradation reaction. To 100 ml of AR-250 dye solution, 200 mg of PNA and ZnO/PNA nanocomposite were added separately and the solution was exposed to UV irradiation in a batch process for 30, 60, 90 and 120 min. For the degradation analysis, of the dye solutions treated with PNA and ZnO/PNA as catalyst, aliquots (10 ml) of dye solution were taken out at regular intervals (5, 10, 20, 30 and 40 min for microwave exposed and 30, 60, 90 and 120 min for UV irradiated). The samples were centrifuged for 10 min

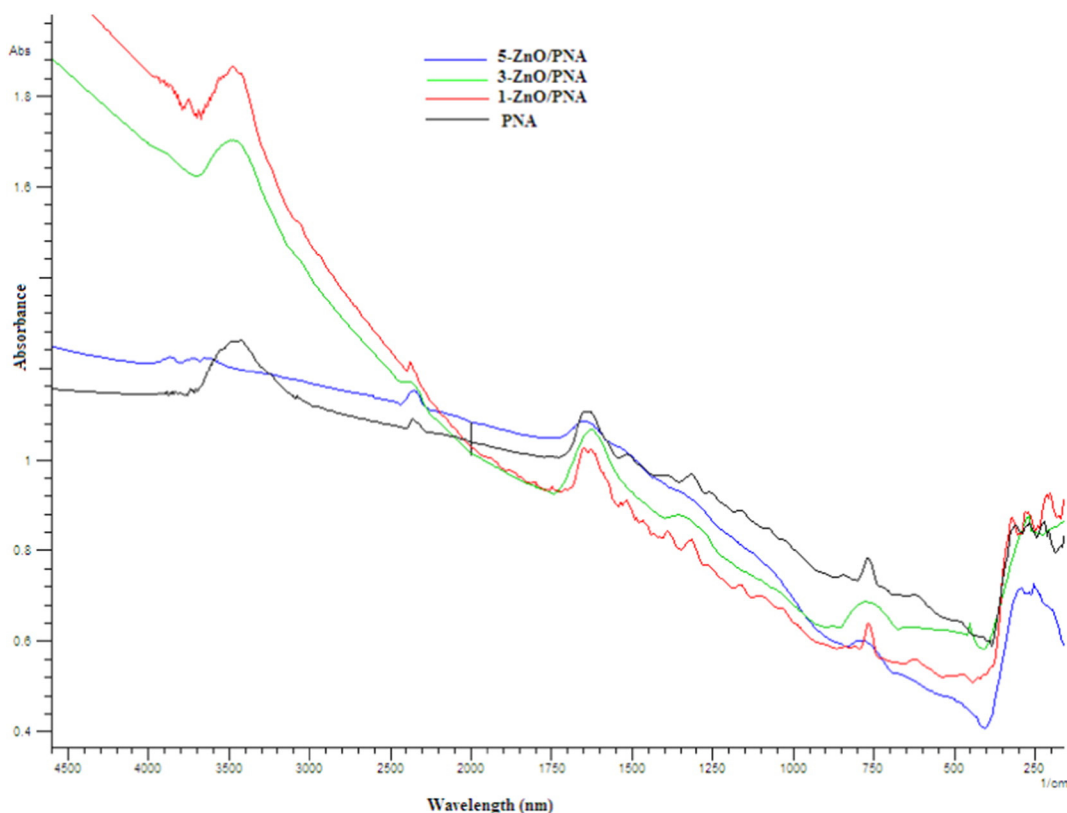


Fig. 1. FTIR spectra of PNA and ZnO/PNA nanohybrids.

at a speed of 5000 rpm and were filtered through a 0.22 μm filter paper (Whatman). The dye concentration was analyzed with a UV–visible spectrophotometer model Shimadzu UV1800 by measuring the change in the absorbance at λ_{max} of AR dye.

3. Characterization

3.1. Spectral analysis

FT-IR spectra of nanocomposites were taken in the form of KBR pellets on FT-IR spectrophotometer model Shimadzu IRA Affinity-1 in the form of KBR pellets. UV–visible spectra were taken on UV–visible spectrophotometer model Shimadzu UV-1800 using NMP as solvent.

3.2. Morphological analysis

X-Ray diffraction patterns of the nanocomposites were recorded on Philips PW 3710 powder diffractometer (Nickel filtered copper Ka radiations). Peak parameters were analyzed through Origin 6.1. The d spacing was calculated using Bragg's equation. Transmission electron micrographs (TEM) were taken on Morgagni 268-D TEM, FEI, USA. The samples were prepared by placing an aqueous drop on carbon-coated copper grid, subsequently drying in air before transferring it to the microscope, operated at an accelerated voltage of 120 kV.

3.3. CV studies

Cyclic voltammetry were taken on DY-2300 series Potentiostat/Biopotentiostat of DIGI-IVY AUSTIN USA, Max. Current Range: (± 10 nA to ± 100 mA in 8 steps), Current Resolution: 0.002% of full scale, with highest resolution of 0.3 A, Potential Range: ± 4.000 V, Bias Potential Range ± 4.000 V (for WE2), Compliance Voltage: $> \pm 10$ V, Input Impedance of electrometer: $> 1012 \Omega$, Potential Bandwidth: > 30 kHz, $\square 20\text{del}/\text{E}$ Low Pass Filter: oC6 ranges (Auto or Manual), depending on sensitivity setting, \square Input Bias Current: < 20 pA @ 25, ADC Sampling Rate: 10 kHz-0.1 Hz, 0.002% resolution, 15,000 data/CH, Cell Control: Purge, Stir, RDE Rotation Control: 0–10 V, \square Electrode configurations: CE, RE, WE (1 CH), or CE, RE, WE1, WE2, Dimensions & Weight: $14.5 \times 24 \times 4.5$ cm, 1 kg, \square Power Requirements: 90–240 VAC, 10 W.

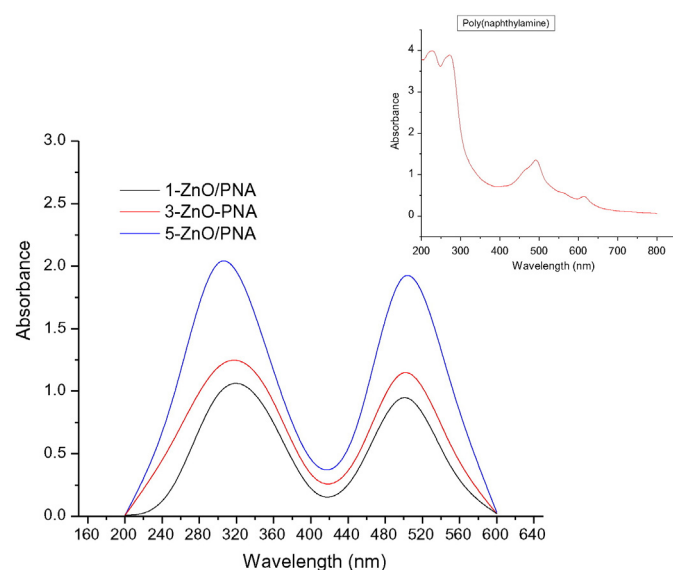


Fig. 2. UV–visible spectra of ZnO/PNA nanocomposites.

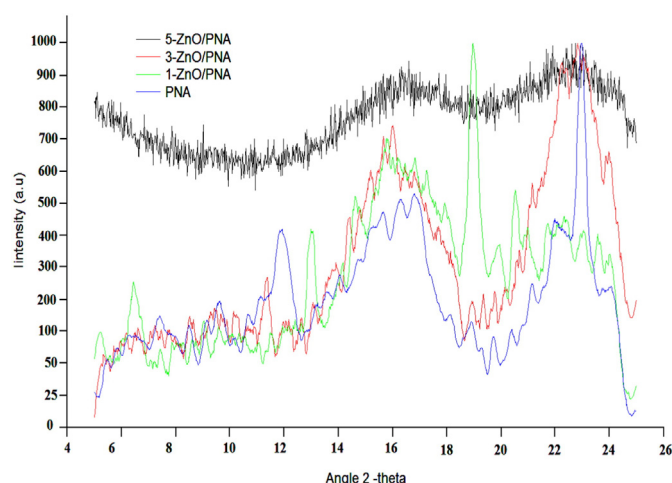


Fig. 3. XRD of PNA and ZnO/PNA nanocomposites.

3.4. LC–MS analysis

For detection and identification of degradation products, liquid chromatography–mass spectroscopy (LC–MS) was conducted using a Finnigan LCQ ion trap mass spectrometer equipped with an electro spray ionization interface (ESI) source and operated in negative polarity mode fitted with a Genesis, C-18 column (4.6×250 mm) containing $4 \mu\text{m}$ packed particles (Alltech, Deerfield, Germany). Acetonitrile and 0.03 M ammonium carbonate buffer, pH 7.7, were used as eluents. The diode array detector allowed for concomitant recording of spectra from 200 to 600 nm. The gradient HPLC separation was coupled with LC/MSD trap 6310, ion trap mass spectrometer (Agilent technologies). The experiments were also carried out in triplicate for evaluating the effect of nanohybrid catalyst dosage and initial dye concentration in the degradation of AR dye.

4. Results and discussion

4.1. Confirmation of formation of PNA and ZnO/PNA nanocomposites by FTIR analysis

The FT-IR spectrum of pure PNA, Fig. 1, revealed an N-H stretching vibration peak centered at 3433 cm^{-1} for secondary amine while the peak at 1633 cm^{-1} was assigned to the imine stretching mode. The peaks at 1508 cm^{-1} and 1429 cm^{-1} and 1411 cm^{-1} were associated with the ring stretching of the quinoid diimine and the benzenoid diamine units at respectively. Other absorption peaks observed were C–N stretching vibration at 1396 cm^{-1} due to the Q-B units and the 1308 cm^{-1} peak due to C–N stretching in B units. The peak at 728 cm^{-1} was produced by C–H out of plane bending. C = C skeletal vibrations, $\nu(\text{C} = \text{C})$ while the absorption peak at 1617 cm^{-1} was correlated to the imine stretching mode. The peaks between 700 and 900 cm^{-1} occurred due to C–H deformation mode and established the position of coupling between two naphthylamine units. The peaks at

Table 1

Analysis of crystallite size and peaks obtained from XRD of PNA and ZnO/PNA nanocomposites.

Nanocomposite	Peak (2θ)	Area $\int \text{adv}$ (peak at 16°)	Height (a.u)	Width (2θ)	Crystallite size (\AA)
PNA	16.14	137	500	1.98	72.9
1-ZnO/PNA	16.02	317	600	2.83	51
3-ZnO/PNA	16.36	357	725	2.80	52
5-ZnO/PNA	16.60	2128	850	4.89	46

769 cm^{-1} and 842 cm^{-1} were consistent with the 1,4 coupling with two and 4 vicinal hydrogen on the two aromatic rings of 1-naphthylamine [29–30]. The peak at 792 cm^{-1} was attributed to 1,5 coupling with three vicinal hydrogen on each benzene ring of naphthylamine. The polymer was therefore confirmed to be a mixture of 1,4 and 1,5 coupled naphthylamine units.

The FT-IR spectrum of 1-PNA-ZnO nanocomposite, revealed the N-H stretching vibration peak for secondary amine at 3437 cm^{-1} while the peak at 1633 cm^{-1} correlated to the imine stretching mode and showed low absorbance of 0.1. The presence of a small hump around 335 cm^{-1} confirmed the presence of ZnO, representing the zinc–oxygen stretching vibration [32]. In case of 3-PNA/ZnO nanocomposite, the spectrum showed a pronounced shift in the N-H stretching vibration for a secondary amine to 3471 cm^{-1} showing an absorbance of 1.7 which was observed to be much higher than for the previous nanocomposite. The peak for the imine stretching mode also showed a shift and was observed at 1624 cm^{-1} while peaks assigned to the ring stretching of the quinoid diimine and the benzenoid diamine units appeared at 1500 cm^{-1} and 1469 cm^{-1} and 1436 cm^{-1} at respectively. The C–N stretching vibration peak due to the quinonoid –benzenoid units was noticed at 1388 cm^{-1} whereas peak due to C–N stretching in benzenoid units appeared at 1346 cm^{-1} . The peak corresponding to the ZnO stretching vibration appeared to be more pronounced and at higher absorbance value as compared to the previous nanocomposite which confirmed higher loading of ZnO in this case. As the loading of ZnO was increased to 5 wt%, the N-H stretching vibration for a secondary amine appeared to reduce showing a lower absorbance value as compared to the previous nanocomposite. However, the imine stretching peak was well formed and so were the peaks corresponding to the polymerization of 1-naphthylamine. The peaks related to the ZnO stretching vibration was also noticed to be highly prominent confirming

the higher loading of ZnO in this case. It can therefore be concluded that with the increase on the loading of ZnO in the nanocomposite, the NH stretching vibration was suppressed due to the interaction of the oxygen of ZnO with the NH of PNA. Interestingly, the peaks corresponding to PNA did not reveal any remarkable shift but only a decrease in the absorbance intensity which clearly confirmed the formation of nanohybrid.

4.2. UV–visible analysis of electronic transitions of PNA and PNA/ZnO nanocomposites

The UV–visible spectrum of PNA in NMP, Fig. 2, revealed peaks at 210 nm, 280 nm in the UV range while the peaks at 500 nm and 610 nm were observed in the visible range. The peaks in the UV range were assigned to $\pi-\pi^*$ transitions while the peaks noticed at 500 nm, 610 nm were attributed to polaronic/bipolaronic transitions as reported by other authors [29–31]. Upon adding 1 wt% ZnO, Fig. 2, the UV spectrum revealed two prominent peaks one at 320 nm and the other at 500 nm. The red shift in the peaks was caused due to the interaction of PNA with ZnO. With the increase in the loading of ZnO, the nanocomposite, 3-ZnO/PNA, revealed further increase in the intensity of the peaks associated with polaronic transitions while maximum intensity was observed for 5-ZnO/PNA. Hence it can be concluded that with the increase in the loading of ZnO upto 5 wt%, the interaction between ZnO with PNA increases due to the formation of intense hydrogen bonds between NH of PNA with O of ZnO that facilitates/enhances delocalization of electrons in the PNA backbone. The band gap of ZnO is reported to be 3.37 eV while that of PNA is 2.11 eV. The closer band gap of the organic–inorganic moieties present in the nanohybrid can promote electron transfer also prevent electron–hole recombination in the UV–visible range as desired for a photocatalyst.

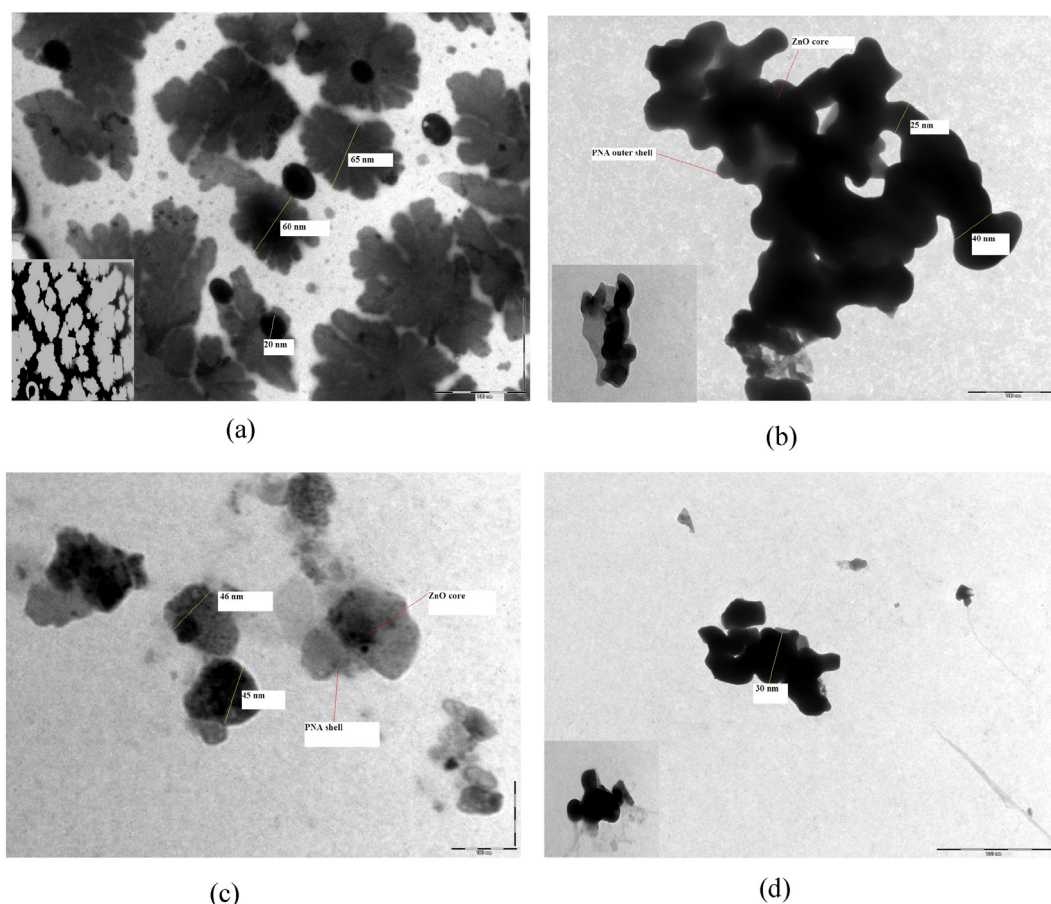


Fig. 4. TEM of (a) Pure PNA, (b) 1-ZnO/PNA (c) 3-ZnO/PNA and (d) 5-ZnO/PNA.

4.3. Confirmation of crystallinity of PNA and ZnO/PNA nanocomposites by XRD analysis

The XRD of pure PNA, Fig. 3, reveals peaks at $2\theta = 11^\circ, 16.3^\circ, 16.5^\circ$ and 23° which shows its semi-crystalline nature. Upon addition of 1 wt% ZnO, Fig. 3, the nanocomposite reveals formation of new peaks at $2\theta = 6.5^\circ, 13.2^\circ$ a broad hump around 16.5° and an intense peak at 19° . The nanocomposite 3-ZnO/PNA, Fig. 3, also reveals similar reordering and reorganization by the presence of new intense peaks at $2\theta = 11.5^\circ$, and two broad humps at $2\theta = 16.5^\circ$ and 23° respectively. Upon further increasing the loading upto 5 wt%, Fig. 3, the nanocomposite exhibits a highly amorphous structure. Thus it can be concluded that with the increase in the loading of ZnO, intense interactions via hydrogen bond formation takes place between the M-O of ZnO with NH of PNA as observed in the UV-visible studies. The integrated area of the peak at 16° corresponding to the characteristic peak of PNA shows \overline{adv} to be 137 which increased when 1 wt% ZnO is loaded in PNA, Table 1. Upon increasing the loading to 3 wt%, the area was observed to be 317 which increased upto 2128 as the loading increased to 5 wt%. Likewise, the crystallite size was observed to decrease with the increase in the loading of ZnO and was observed to be 46 Å in case of 5-ZnO/PNA. This shows that upon loading of ZnO, the particle size decreased leading to an increase in the surface area which can also be corroborated from the TEM analysis discussed in the upcoming section.

4.4. Morphological analysis of PNA and ZnO/PNA nanocomposites

The TEM of PNA, Fig. 4(a), showed a self-assembled morphology. The particle size was calculated to be 20–65 nm. The PNA particles revealed the formation of a flower-like morphology with several leaf-like petals. The TEM image of 1-PNA/ZnO, Fig. 4(b), showed typical core-shell morphology where the dense ZnO particles appeared to reside in the PNA core. The size of these nanoparticles was found to be in the range of 25–40 nm. The 3-PNA/ZnO Fig. 4(c), nanocomposite revealed formation of a sea-shell-like structure showing a core-shell morphology in this case as well; ZnO being the dense core and PNA the outer shell. The size of these nanoparticles was found to be in the range of 40–45 nm. With the increase in the loading upto 5 wt%, Fig. 4(d), the morphology changed to a dense core like structure showing distinct dark and bright regions of ZnO core and PNA shell. The particle size was noticed to be in the range of 30 nm. It can be concluded that the PNA particles cover the ZnO core nanoparticles to form a distorted spherical morphology. Ultrasonic-assisted synthesis of PNA produces self-assembled morphology and its nanocomposites with PNA form a distorted core-shell structure. The denseness of the core increases with the increase in the loading of ZnO in PNA. The nanocomposites exhibit agglomeration which is found to increase with the increase in the loading of ZnO in PNA matrix.

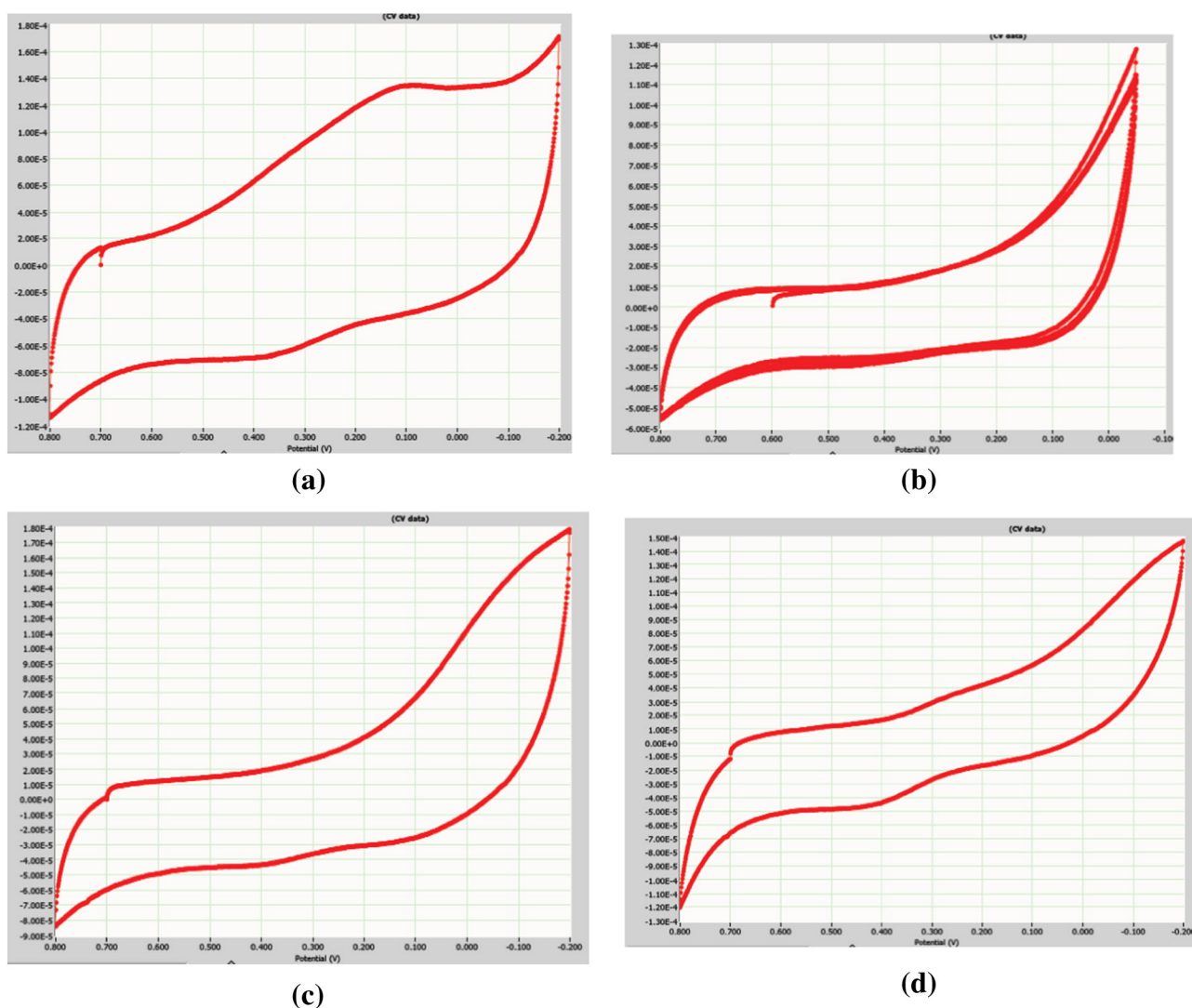


Fig. 5. Cyclic voltammogram of (a) PNA, (b) 1-PNA/ZnO, (c) 3-PNA/ZnO and (d) 5-PNA/ZnO.

4.5. Cyclic voltammetry studies

The cyclic voltammogram of pure PNA, Fig. 5(a), exhibited an oxidation peaks at 0.7 and 0.1 V while the reduction peak was observed at 0.35 V and 0.1 V respectively. The peaks observed were not sharp and also confirmed that the oxidation and reduction were irreversible in PNA. The nanocomposite 1-PNA/ZnO, Fig. 5(b), showed only one oxidation peak at 0.7 V while 2 reduction peaks were observed at 0.45 V and 0.1 V respectively. Likewise for 3-PNA/ZnO, Fig. 5(c), the oxidation peak was observed at 0.7 V while reduction peak was found at 0.1 V and 0.4 V respectively. The 5-PNA/ZnO nanocomposite, Fig. 5(d), showed similar oxidation peak as observed incase of the other two nanocomposites at 0.7 V while the reduction peak appeared at 0.4 V. The results revealed that loading of ZnO caused a slight shift in the reduction peaks of the nanocomposites as compared to pure PNA. The HOMO energy was calculated to be -5.5 eV for all the samples while the LUMO energy was observed to vary from -4.5 – 5 eV.

4.6. Dye degradation studies

The degradation of AR dye solution was monitored spectrophotometrically upon exposure to microwave irradiation for 40 min and under UV irradiation for 120 min respectively in presence of PNA and ZnO/PNA as catalyst. The UV–visible spectrum of PNA-250 solution upon exposure to microwave irradiation for 40 min showed a decrease in the characteristics absorbance peaks at 300 nm and 500 nm. The peak at 300 nm were assigned to π - π^* transitions of the benzene ring in AR dye while the peak at 500 nm was associated with that of substituted benzene. As the exposure time increased from 5 to 40 min, the absorbance maxima decreased in both the peaks. The peak at 300 nm showed a decrease in the absorbance value from 1.4 in 5 min to 0.6 in 40 min. Likewise, the peak at 500 nm showed a decrease from 1.7 to 1.0 in 40 min. The spectra of PNA-250, upon exposure to UV irradiation also showed significant reduction in the absorbance values i.e. from 1.4 in 30 min to 0.8 in 120 min incase of the peak observed at 300 nm while the peak at 500 nm shows a decrease from 1.6 to 1.0 in 120 min. The UV–visible spectrum of 1-ZnO/PNA-AR-250 also revealed a decrease in the absorbance value from 1.5 to 0.3 in 40 min for the peak at 300 nm while for the 500 nm peak, the absorbance values showed a decrease from 1.2 to 0.4 in 40 min. Similarly, for UV irradiated 1-ZnO/PNA-AR-250 solution, the decrease in the absorbance of 300 nm peak was noticed from 1.5 to 0.6 in 120 min and for the 500 nm peak, the absorbance values decreased from 1.0 to 0.6 in 120 min (supplementary information). The decrease in the absorbance intensity of the peaks in the UV and visible region thus confirmed the degradation of the AR dye. It appeared that under microwave irradiation, upon addition of ZnO/PNA, the decrease in the absorbance intensity of the peak in the visible region was enhanced which confirmed the catalytic behaviour of the nanohybrid under microwave-irradiation. Hence it can be concluded that dye degradation was enhanced when ZnO/PNA nanocomposite was used as a catalyst under microwave irradiation. Under UV irradiation, the degradation time taken was three times slower than the time taken under microwave irradiation. As compared to pristine PNA, the rate of degradation under microwave irradiation was enhanced using ZnO/PNA as catalyst. The mechanism is explained in the later section.

4.7. Comparison of degradation kinetics

The plot of C/C_0 vs. time using PNA as catalyst under microwave irradiation, Fig. 6(a), showed 35% degradation for the 300 nm peak while for 500 nm peak, degradation was observed to be 25%. Similarly, for PNA as photocatalyst under UV irradiation, Fig. 6(b), the % degradation was observed to be 40% and 36% respectively. Under microwave irradiation, when the nanocomposite 1-ZnO/PNA was used as catalyst, higher degradation was observed Fig. 6(a). In presence of the nanocomposite,

the 300 nm peak, revealed 75% degradation while the 500 nm peak revealed 85% degradation. Likewise when the nanocomposite was used as a photocatalyst, under UV irradiation, Fig. 6(b), the 300 nm peak, revealed 60% degradation while 50% degradation was noticed for the 500 nm peak. The plots of $\ln C/C_0$ vs. time, Fig. 7 (a), (b) revealed the degradation kinetics of AR dye degradation using PNA and 1-ZnO/PNA as catalysts under microwave and UV irradiation respectively. The kinetics was found to be of first order in all the cases. The rate constant (k) values using PNA as catalyst under microwave irradiation were observed to be 0.009 and 0.007 for 300 nm and 550 nm peaks respectively. The k values for UV exposed solutions using the same catalyst, were calculated to be 0.005 and 0.004 for the 300 nm and 500 nm peaks respectively. Hence the kinetics of degradation under microwave was twice as fast as compared to UV light irradiation. Using ZnO/PNA as catalyst under microwave irradiation, Fig. 7 (a), the rate constant values were observed to be 0.052 and 0.036 for the 300 nm and 500 nm peaks respectively while under UV irradiation using the same catalyst, the rate constant values were observed to be 0.009 and 0.007 for the 300 nm and 500 nm peaks respectively. The kinetics of degradation was noticed to be higher under microwave than under UV irradiation and remarkably high when ZnO/PNA was used as catalyst.

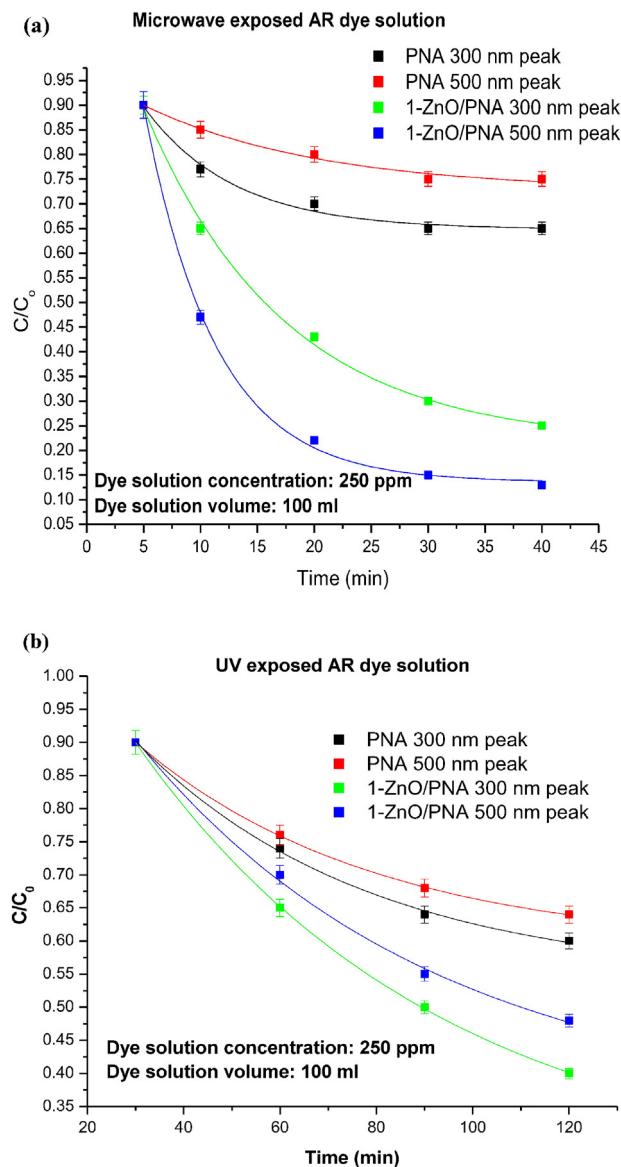


Fig. 6. C/C_0 vs. time plot for AR dye solution containing PNA and 1-ZnO/PNA as catalyst exposed to (a) microwave irradiation (b) UV irradiation.

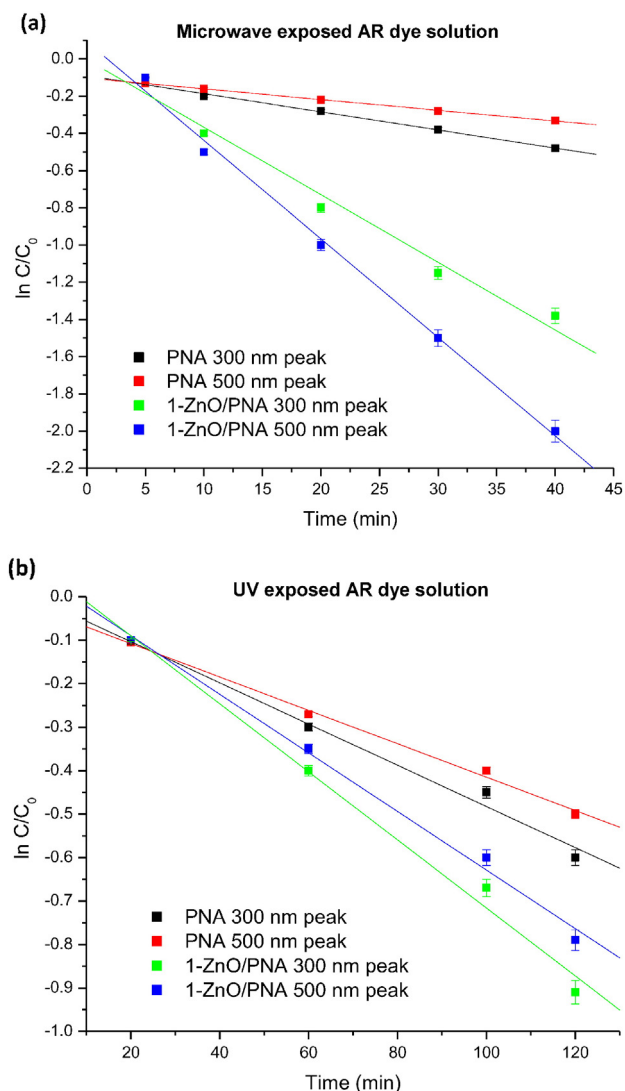


Fig. 7. In C/C₀ vs. time plot for AR dye solution containing PNA and 1-ZnO/PNA as catalyst exposed to (a) microwave irradiation (b) UV irradiation.

4.8. Proposed mechanism and degradation pathway

Catalytic degradation of the dye, occurs through involvement of OH[•] and H[•] free radicals. It has been extensively reported that the hydroxyl radicals (•OH) are generated during microwave as well as photocatalytic degradation reactions and to confirm the presence of •OH radicals, a solution of terephthalic acid (TA) (1×10^{-4} M) in 0.1 M NaOH was used [33–35]. TA reacts with •OH to produce highly fluorescent 2-hydroxyterephthalic acid which gives an emission peak at 415 nm upon excitation at wavelength of 315 nm. As can be seen in Fig. 8 (a), the fluorescence intensity of the 2-hydroxyterephthalic acid increased upon increase in the exposure time of microwave irradiation. Similar behavior was observed with UV irradiation, Fig. 8(b). Interestingly, the fluorescence intensity upon microwave irradiation increased twice as high as compared to UV irradiation which confirmed higher generation of •OH under microwave irradiation. The area under the peak of TA was compared to investigate the extent of radical formation with time. It was found that the area under the peak for microwave degraded samples increased from 22,617 in 10 min to 38,586 in 40 min. Similarly the area under the peak for UV degraded samples increased from 12,114 in 30 min to 21,085 in 120 min. Interestingly the •OH under microwave irradiation was higher than under UV irradiation which is evident from the area under the peaks in the two cases. The •OH radicals

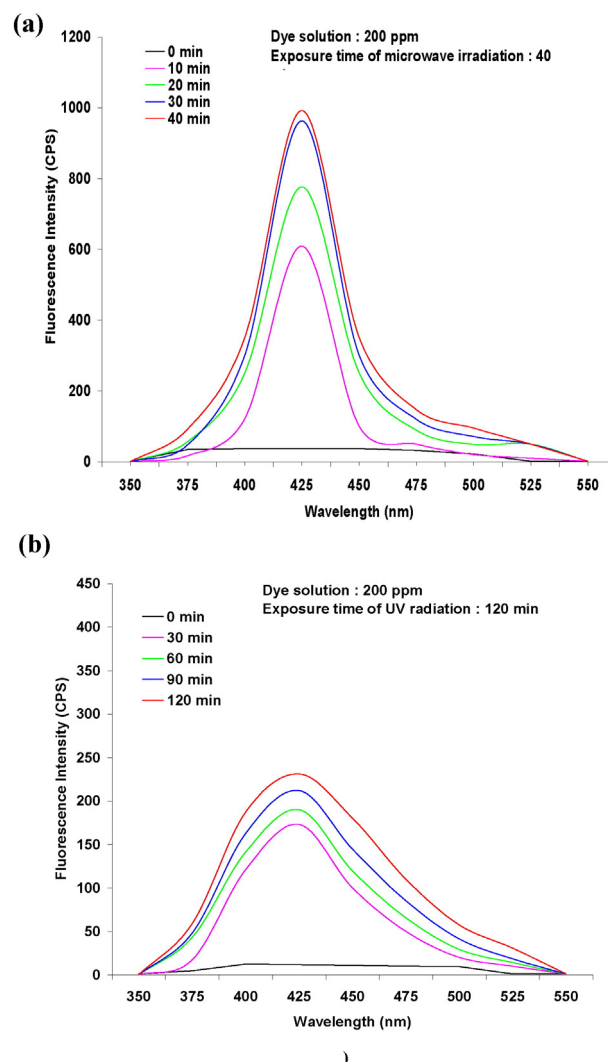


Fig. 8. Variation of fluorescence intensity of 2-hydroxy terephthalic acid upon (a) microwave exposure (b) UV light exposure.

generated upon microwave irradiation in 10 min were observed to be higher than those generated upon UV exposure in 120 min. Hence it can be concluded that •OH radicals were produced in higher amount upon microwave exposure in a short time span of 10 min which can be correlated to non thermal effect observed in microwave heating [31]. In presence of a polar solvent like H₂O, microwave radiation produces high temperature known as “thermal effect” through dielectric heating which splits into H₂ and O₂. Since effective charge separation occurs under microwave irradiation in PNA, it produces sufficient electrons and holes that can get transferred to the VB and CB of ZnO and therefore sensitize it. Horikoshi et al. [24–26] have observed non-thermal effect of microwave radiation in enhancing the rate of dye degradation in several studies. The band gap of ZnO is reported to be 3.37 eV while that of PNA is 2.11 eV. Therefore, upon exposure to microwave irradiation, electrons from PNA get excited and charge carriers are created.

The degraded fragments were analyzed using LCMS technique. At similar retention time, LCMS results revealed 4 peaks as shown in Table 2. The first intermediate with 100% abundance was taken as the main degradation product/the parent dye P1, while intermediates with low m/z values, (123–56) were labelled as F1– F10 as shown in Scheme 1. Above m/z 149, no prominent intermediate was found. F1 was taken as the intermediate from parent dye PI which generates intermediates from m/z 149–m/z 56. The intermediates revealed that

Table 2
Fragments obtained at 20 min retention time.

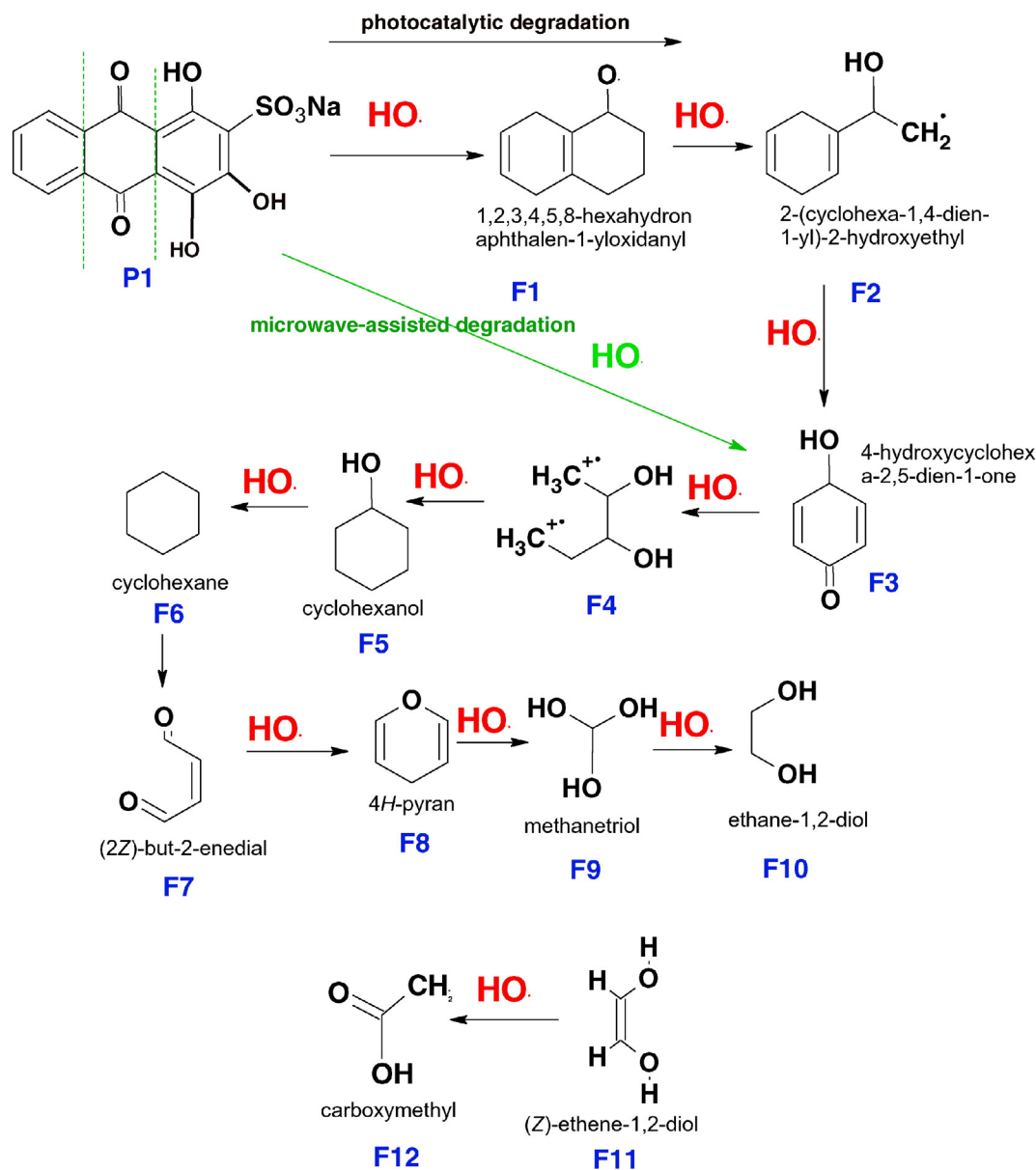
Sample code	Relative intensity (%)
PNA/ZnO (microwave)	62(100%), 84(25%), 104(40%), 110(15%)
PNA (microwave)	82(100%), 100(30%), 60 (15%), 62(12%)
PNA (photocatalysis)	82(100%), 100(90%), 64(66%), 60(55%), 123(30%), 56(20%)
PNA/ZnO (Photocatalysis)	100(100%), 149(70%), 59(35%), 62(30%)

degradation proceeded via elimination of sulphonate group, followed by its oxidation by OH^\bullet free radicals, and attack on carbons of naphthalene ring resulting in its cleavage and oxidation. The intermediate F1 (m/z 149) [1,2,3,4,5,8-hexahydronaphthalen-1-yloxidanyl] was obtained from parent dye P1 by elimination of one SO_3Na group at C4 which degraded to F2 (m/z 123), by cleavage of benzene ring resulting into the formation of 2-(cyclohexa-1,4-dien-1-yl)-2-hydroxyethyl. This intermediate further degraded to F3 (4-hydroxycyclohexa-2,5-dien-1-one) by reaction with OH^\bullet free radicals and formed F4 that converted to cyclohexanol (F5) (m/z 100) which was observed to be the major

degraded product of UV catalyzed reaction. Cyclohexanol further degraded to form cyclohexane (F6) (m/z 84) which was found to be a minor fragment in microwave assisted degradation using ZnO/PNA and its further degradation produced (2Z)-but-2-enal (F7) (m/z 84) which was a major product obtained in microwave-assisted degradation using ZnO/PNA. However, using PNA as catalyst, 4H-pyran (m/z 82), F8 was formed as a major product which further degraded to form F9 methanetriol (m/z 64) as a major product of UV catalyzed reaction using PNA as catalyst. Using ZnO/PNA as catalyst, F10 ethane-1,2-diol (m/z 62) was obtained which transformed to F11 ethane-1,2-diol (m/z 60) and eventually converted to F12 carboxymethyl (m/z 59) and finally to F13 2-hydroxyprop-1-en-1-ylidene (m/z 56). Based on these observations, it can be concluded that microwave irradiation degraded the AR dye into intermediates with low molar masses like ethanediol that are non-toxic in nature.

5. Conclusion

ZnO/PNA nanocomposites were successfully synthesized and FTIR studies established the formation of an organic–inorganic hybrid



Scheme 1. Degradation pathway.

nanocomposite while UV confirmed the presence of polaronic state in PNA. TEM of the nanocomposites confirmed the formation of core-shell morphology showing distinct dense ZnO core and PNA outer shell with particle size ranging from 20 to 45 nm. Preliminary degradation studies of AR dye solution were monitored by UV–visible analysis. It was noticed that under microwave irradiation, the rate of degradation was faster as compared to UV irradiation. As compared to pristine PNA, the rate of degradation of AR dye solution under microwave irradiation was enhanced using ZnO/PNA as catalyst. AR dye revealed 90% degradation in presence of the nanocomposite catalyst within 40 min. Although, both techniques revealed kinetics of degradation to be of first order, microwave degradation was found to be twice as fast as photocatalytic degradation. When ZnO/PNA was used as a catalyst under microwave irradiation, the k values were observed to be 0.052 and 0.036 for the 300 nm and 500 nm peaks respectively. The same catalyst when exposed to UV irradiation showed rate constant values as 0.009 and 0.007 corresponding to the 300 nm and 500 nm peaks respectively. The \bullet OH radical generation was confirmed by measuring the fluorescence intensity of 2-hydroxyterephthalic acid which was found to increase remarkably for dye solutions exposed microwave irradiation. LCMS analysis revealed that the fragments obtained by microwave degradation were potentially nontoxic in nature. The study therefore, demonstrates the feasibility of using ZnO/PNA as a microwave catalyst for rapid and eco-friendly degradation of dyes.

Acknowledgments

The corresponding author, Dr. Ufana Riaz, also wishes to acknowledge the University Grants Commission (UGC), India, for granting major research projects via sanction no. F. No. 41–199/2012(SR). The author also wishes to acknowledge the sophisticated analytical instrumentation facility at All India Institute of Medical Sciences (AIIMS), for granting TEM facility.

References

- [1] U. Riaz, S.M. Ashraf, J. Kashyap, Enhancement of photocatalytic properties of transitional metal oxides using conducting polymers: a mini review, *Mater. Res. Bull.* 71 (2015) 75–90.
- [3] P. Chowdhury, J. Moreira, H. Goma, A.K. Ray, Visible-solar-light-driven photocatalytic degradation of phenol with dye-sensitized TiO₂: parametric and kinetic study, *Ind. Eng. Chem. Res.* 51 (12) (2012) 4523–4532.
- [4] K. Pandiselvi, S. Thambidurai, Synthesis of porous chitosan–polyaniline/ZnO hybrid composite and application for removal of reactive orange 16 dye, *Colloids Surf. B Biointerfaces* 108 (2013) 229–238.
- [5] Z. Pei, L. Ding, M. Lu, Z. Fan, S. Weng, J. Hu, P. Liu, Synergistic Effect in Polyaniline–Hybrid Defective ZnO with Enhanced Photocatalytic Activity and Stability, *J. Phys. Chem. C* 118 (18) (2014) 9570–9577.
- [6] Y. Peng, J. Ji, Y. Zhang, H. Wan, D. Chen, Preparation of Poly(m-phenylenediamine)/ZnO Composites and Their Photocatalytic Activities for Degradation of C.I. Acid Red 249 under UV and Visible Light Irradiations, *Environ. Prog. Sustainable Energy* 33 (2014) 123–130.
- [7] R. Qiu, D. Zhang, Y. Mo, L. Song, E. Brewer, X. Huang, Y. Xiong, Photocatalytic activity of polymer-modified ZnO under visible light irradiation, *J. Hazard. Mater.* 156 (1–3) (2008) 80–85.
- [8] A. Saffar-Teluri, S. Bolouk, M. Amini, Synthesis of ZnO microcrystals and their photocatalytic ability in the degradation of textile azo dyes, *Res. Chem. Intermed.* 39 (2013) 3345–3353.
- [9] Y. Zheng, C. Chen, Y. Zhan, X. Lin, Q. Zheng, K. Wei, J. Zhu, Y. Zhu, Luminescence and photocatalytic activity of ZnO nanocrystals: correlation between structure and property, *Inorg. Chem.* 46 (2007) 6675–6682.
- [10] Y. Li, W. Xie, X. Hu, G. Shen, X. Zhou, Y. Xiang, X. Zhao, P. Fang, Comparison of dye photodegradation and its coupling with light-to-electricity conversion over TiO₂ and ZnO, *Langmuir* 26 (2009) 591–597.
- [11] Q. Li, C. Zhang, J. Li, Photocatalysis and wave-absorbing properties of polyaniline/TiO₂ microbelts composite by in situ polymerization method, *Appl. Surf. Sci.* 257 (2010) 944–948.
- [12] M.A. Salem, A.F. Al-Ghonemiy, A.B. Zaki, Photocatalytic degradation of allura red and quinoline yellow with polyaniline/TiO₂ Nano composite, *Appl. Catal. B Environ.* 91 (2009) 59–66.
- [13] L. Su, Y.X. Gan, Experimental study on synthesizing TiO₂ nanotube/polyaniline (PANI) nanocomposites and their thermoelectric and photosensitive property characterization, *Compos. Part B* 43 (2012) 170–182.
- [14] H. Zhang, R. Zong, Y. Zhu, Photocorrosion inhibition and photoactivity enhancement for zinc oxide via hybridization with monolayer polyaniline, *J. Phys. Chem. C* 113 (2009) 4605–4611.
- [15] L. Zhang, P. Liu, Z. Su, Preparation of PANI TiO₂ nanocomposites and their solid-phase photocatalytic degradation, *Polym. Degrad. Stab.* 91 (2006) 2213–2219.
- [16] U. Riaz, S.M. Ashraf, M. Aqib, Microwave-assisted degradation of acid orange using a conjugated polymer, polyaniline, as catalyst, *Arab. J. Chem.* 7 (1) (2014) 79–86.
- [17] U. Riaz, S.M. Ashraf, A. Madan, Effect of microwave irradiation time and temperature on the spectroscopic and morphological properties of nanostructured poly(carbazole) synthesized within bentonite clay galleries, *New J. Chem.* 38 (2014) 4219–4228.
- [18] U. Riaz, S.M. Ashraf, S. Kumar, I. Ahmad, Controlling the growth of polycarbazole within the silicate galleries using peroxides via microwave-assisted green synthesis, *Chem. Eng. J.* 241 (2014) 259–267.
- [19] U. Riaz, S.M. Ashraf, Microwave-Assisted Solid State in Situ Polymerization and Intercalation of Poly(carbazole) between Bentonite Layers: Effect of Microwave Irradiation and Gallery Confinement on the Spectral, Fluorescent, and Morphological Properties, *J. Phys. Chem. C* 116 (22) (2012) 12366–12374.
- [20] U. Riaz, S.M. Ashraf, Effect of solid state intercalation conditions in controlling the self-assembled nanostructured polycarbazole–montmorillonite nanocomposites synthesized by mechano-chemical and microwave-assisted techniques, *Appl. Clay Sci.* 52 (2011) 179–183.
- [21] A. Kajbafvala, H. Ghorbani, A. Paravar, J.P. Samberg, E. Kajbafvala, S.K. Sadrnezhad, Effects of morphology on photocatalytic performance of zinc oxide nanostructures synthesized by rapid microwave irradiation methods, *Superlattice. Microsc.* 51 (4) (2012) 512–522.
- [22] S. Islam, M.R. Karim, M.B. Zaman, Shape controllable preparation and characterization of submicron lamellar and rod clusters of zinc oxide via conventional and microwave accelerated reaction methods, *Mater. Lett.* 92 (1) (2013) 376–378.
- [23] N.P. Herring, K.A. Zeid, M.B. Mohamed, J. Pinski, M.E. Shall, Formation Mechanisms of Gold–Zinc Oxide Hexagonal Nanopyramids by Heterogeneous Nucleation using Microwave Synthesis, *Langmuir* 27 (24) (2011) 15146–15154.
- [24] S. Horikoshi, T. Nishimura, H. Tsutsumi, N. Serpone, Microwave Discharge Electrodeless Lamps (MDELs). Part VIII. Continuous On-Site Solar Energy Remediation of Contaminated Water, *Chem. Eng. Technol.* 39 (1) (2016) 102–107.
- [25] S. Horikoshi, H. Tsutsumi, H. Matsuzaki, A. Furube, A.V. Emelinec, N. Serpone, *In situ* picosecond transient diffuse reflectance spectroscopy of opaque TiO₂ systems under microwave irradiation and influence of oxygen vacancies on the UV-driven/microwave-assisted TiO₂ photocatalysis, *J. Mater. Chem. C* 3 (2015) 5958–5969.
- [26] S. Horikoshi, N. Serpone, On the influence of the microwaves' thermal and non-thermal effects in titania photo-assisted reactions, *Catal. Today* 224 (2014) 225–235.
- [27] S. Horikoshi, N. Serpone, Coupled microwave/photoassisted methods for environmental remediation, *Molecules* 19 (11) (2014) 18102–18128.
- [28] S. Horikoshi, Y. Minatodani, H. Tsutsumi, H. Uchida, M. Abe, N. Serpone, Influence of lattice distortion and oxygen vacancies on the UV-driven/microwave-assisted TiO₂ photocatalysis, *J. Photochem. Photobiol. A Chem.* 265 (1) (2013) 20–28.
- [29] U. Riaz, S.M. Ashraf, Latent photocatalytic behavior of semi-conducting poly(1 naphthylamine) nanotubes in the degradation of comassie brilliant blue RG, *Sep. Purif. Technol.* 95 (10) (2012) 97–102.
- [30] U. Riaz, S.M. Ashraf, Semi-conducting poly(1-naphthylamine) nanotubes: a pH independent adsorbent of sulfonate dyes, *Chem. Eng. J.* 174 (2–3) (2011) 546–555.
- [31] U. Riaz, S.M. Ashraf, Synergistic effect of microwave irradiation and conjugated polymeric catalyst in the facile degradation of dyes, *RSC Adv.* 4 (2014) 47153–47162.
- [32] S.M. Hosseini, I. Abdolhosseini Sarsari, P. Kameli, H. Salamati, Effect of Ag doping on structural, optical, and photocatalytic properties of ZnO nanoparticles, *J. Alloys Compd.* 640 (2015) 408–415.
- [33] K. Bubacz, E. Kusiak-Nejman, B. Tryba, A.W. Morawski, Investigation of OH radicals formation on the surface of TiO₂/N photocatalyst at the presence of terephthalic acid solution. Estimation of optimal conditions, *J. Photochem. Photobiol. A Chem.* 261 (1) (2013) 7–11.
- [34] Y. Nakabayashi, Y. Nosaka, The pH dependence of OH radical formation in photoelectrochemical water oxidation with rutile TiO₂ single crystals, *Phys. Chem. Chem. Phys.* 17 (2015) 30570–30576.
- [35] Y. Nosaka, S. Komori, K. Yawata, T. Hirakawaa, A.Y. Nosaka, Photocatalytic \bullet OH radical formation in TiO₂ aqueous suspension studied by several detection methods, *Phys. Chem. Chem. Phys.* 5 (2003) 4731–4735.